



Bending Performance of Epoxy Adhesive Joints of Prefabricated Concrete Elements

Hongbo Peng^{1,2}, Zhongya Zhang^{1,2}, Yang Zou^{1,2*}, Jincen Guo^{1,2}, Xiaoyan Zhang^{1,2} and Xingqi Zeng^{1,2}

¹State Key Laboratory of Mountain Bridge and Tunnel Engineering, Chongqing Jiaotong University, Chongqing, China, ²School of Civil Engineering, Chongqing Jiaotong University, Chongqing, China

OPEN ACCESS

Edited by:

Zhigang Zhang,
Chongqing University, China

Reviewed by:

Kangkang Wang,
CCCC Highway Consultants Co., Ltd.,
China

Yang Wei,
Nanjing Forestry University, China

*Correspondence:

Yang Zou
zouyang@cqjtu.edu.cn

Specialty section:

This article was submitted to
Structural Materials,
a section of the journal
Frontiers in Materials

Received: 21 January 2022

Accepted: 28 February 2022

Published: 07 April 2022

Citation:

Peng H, Zhang Z, Zou Y, Guo J,
Zhang X and Zeng X (2022) Bending
Performance of Epoxy Adhesive Joints
of Prefabricated Concrete Elements.
Front. Mater. 9:859532.
doi: 10.3389/fmats.2022.859532

The assembly construction of prefabricated UHPC elements can well balance quality reliability and construction convenience, thus it has excellent application prospects in bridge engineering. The joints between prefabricated elements are the key to ensuring the overall force performance of the structure, which directly determine the load-bearing capacity and the life of structure. To clarify the bending behavior of epoxy adhesive joints between prefabricated UHPC elements, four groups of 12 bending tests were carried out with different interface treatment forms as parameters. The failure modes, load-deflection curves, and ultimate bending strength of the interface were investigated. The results reveal that the interfacial failure modes mainly include the interfacial stripping failure of epoxy-UHPC surface, steel fibers and fine aggregates into UHPC surface by pulling out, and tensile damage of UHPC at the root of key teeth on the side of the keyway interface. The load-deflection curves of all specimens exhibit the two-fold lines form. The load tends to rise linearly during the loading phase, and there is no yielding phase before the failure. The load-carrying capacity of the specimen is lost immediately after the failure, and no reliable residual strength is available except for the keyway interface. In addition, the bending strength of rough interface, groove interface, and keyway interface are respectively improved by -24.02, 2.34, and 4.64%, compared with the natural interface. So it is recommended that the joint between prefabricated UHPC elements take the form of keyway interface. Finally, a simplified force model of the keytooth adhesive joint is proposed, and a calculation formula for the flexural bearing capacity is established based on the principal of Mohr's circle, based on the experimental results and theoretical analysis. The mean ratio of the proposed adhesive joint calculation equation to the experimental results was 0.925 with a standard deviation of 0.065.

Keywords: ultra-high performance concrete, epoxy resin, prefabricated assembly, bending performance, experimental study

INTRODUCTION

Normal concrete has been widely used because of its advantages of easy material extraction, good moldability and high compressive strength, but it also has the disadvantages of low tensile strength, difficult to control the crack width after cracking and obvious brittle characteristics. To improve the brittle properties of normal concrete and limit its crack development, a large majority of scholars and

researchers at home and abroad have developed high performance fiber reinforced concrete, represented by ultra-high performance concrete (UHPC) and engineered cementitious concrete (ECC). ECC has the obvious strain-hardening characteristics, high tensile and compressive toughness, excellent durability, good deformation capacity and energy dissipation capacity. The application of this material in buildings, bridges and other structures can meet the safety, applicability and durability requirements. Qin et al. (Qin et al., 2020) applied high strength, high ductility ECC to strengthen reinforced concrete beams and investigated its flexural properties. The test results show that when the beam reaches its ultimate state, no local cracking occurs in tensile zone, but more micro-cracks appear due to the high toughness of ECC. In addition, the cracking load, yield load, ultimate load, ductility and energy absorption capacity are improved. Zhang et al. (Zhang et al., 2020; Zhang et al., 2021) developed the high strength, high ductility ECC with substitution of fly ash and cement by rice husk ash to enrich the variety of ingredients in ECC and make ECC more eco-friendly. In addition, to realize self-healing and increase the strength of ECC, Zhang et al. (Zhang et al., 2022) investigated the mechanical properties of ECC with the addition of vegetative bacterial cells. The results show that the compressive, cracking and tensile strength of ECC are increased, but the tensile strain capacity is slightly decreased due to the addition of bacteria.

UHPC is a fiber-reinforced cementitious composite material with a compressive strength of 150 MPa or more and excellent mechanical properties, durability, and toughness (De Larrard and Sedran, 1994; Wille et al., 2011; Wang et al., 2015; Xue et al., 2020; Du et al., 2021). The steel fibers into UHPC inhibit the sprouting and development of cracks, thereby enhancing their tensile properties (Liew, 2015; Lee et al., 2017; Meng and Khayat, 2017). In addition, the dense matrix microstructure provides high resistance to the intrusion of harmful chemical ions (Cl^- , SO_4^{2-} , etc.) and CO_2 , resulting in strong resistance to permeation, carbonation, corrosion, and freeze-thaw cycles, and exhibiting excellent durability performance (Meng et al., 2018; Meng and Khayat, 2018; Qi et al., 2019). UHPC is considered to be one of the most promising construction materials (Zhou et al., 2018; Cheng et al., 2021; Lian et al., 2021), and a majority of scholars have conducted studies on its application in bridge engineering structures, including piers, main girders, deck slabs, arches, bridge joints, and old bridge reinforcement (Chen et al., 2016; Haber et al., 2018; Ren et al., 2019; Su et al., 2019). The results show that the application of UHPC in bridge structures is expected to solve many technical challenges of existing conventional bridge structures. For example, UHPC-based bridge structures can significantly reduce the section size, effectively reduce the self-weight of the structure, and thus improve the spanning capacity of the structure (Zhu et al., 2020). Due to its excellent crack-resistance performance (Li and Deng, 2021), UHPC can also be applied in crack-prone structures such as concrete deck slabs in hogging moment zones to meet the requirements of tensile and crack resistance. UHPC applied in orthotropic steel decks can significantly increase the stiffness of structures and mitigate the problems of fatigue

cracking and pavement vulnerability of steel bridge decks (Dieng et al., 2013; Abdelbaset et al., 2020; Wang et al., 2021; Abdelbaset et al., 2022).

However, UHPC has a risk of early cracking due to internal self-drying and chemical shrinkage during the setting and hardening process, which can cause self-shrinkage and is usually greater than $800 \mu\epsilon$ (Yoo et al., 2014; Huang and Ye, 2017). In addition, high-temperature steam curing is an important part of the preparation of UHPC, which can improve the strength of concrete and give it excellent durability while reducing the later shrinkage. However, on-site steam curing increases the construction difficulty and cost significantly in practical engineering (Garas et al., 2009). Based on the above problems, the assembled construction of prefabricated UHPC elements can effectively solve the problems of large self-shrinkage and difficult steam curing of UHPC in cast-in-place construction and has a promising application in the rapid construction technology of assembled bridges and large-span bridge structures. Shao et al. (Shao et al., 2019) proposed three types of high-performance assembled bridge structures based on UHPC, including assembled box girder structures, fully prefabricated UHPC " π " shaped girders, and fully prefabricated steel-UHPC lightweight composite " π " shaped girders. A large quantity of experimental research and theoretical analysis shows that the self-weight of assembled UHPC bridge structures can be reduced to 40–50% of that of traditional structures under equal strength-bearing conditions. Its great transportation convenience can facilitate the rapid construction of large elements. Moreover, the size of joints between each girder on-site can be significantly reduced, significantly reduces the on-site work. Wang et al. (Wang et al., 2019) proposed a steel-prefabricated UHPC composite beam with full dry connection and carried out two full-scale beam tests combined with finite element numerical analysis to investigate the flexural and crack-resistance performance of composite beam.

In the prefabricated UHPC assembly structure, the joints can make it have better force transmission performance and ensure its impermeability and integrity. At present, the joints can be divided into three types according to the connection material at the joints: the dry joints with direct contact on the surface of the joints, the wet joints with filled concrete or mortar, and the glued joints with epoxy resin. Dry joints are banned by the AASHTO due to the disadvantages of not providing effective durability protection for post-tensioned prestressing tendons, and it is suggested that only glue joints or wet joints can be used in all precast assembled concrete structures. Pan et al. (Pan et al., 2016) compared the flexural performance of five novel wet joints of steel-RPC composite deck slabs. Since steel fibers improve the performance of the RPC layer after cracking, a durability-based RPC tensile stress is recommended to replace the initial cracking stress for a more economical deck panel design. Shao et al. (Shao et al., 2013; Shao et al., 2017) demonstrated that the crack-resistance performance of steel-plate enhanced wet joints and reinforcement-enhanced wet joints was better than conventional wet joints by bending tests on steel-RPC composite deck slabs. Xiao et al. (Xiao et al., 2022) conducted

TABLE 1 | Mix ratio of UHPC.

Components	Mass ratio	Proportion (%)
Cement	1.000	34.55
Silica fume	0.250	8.64
Quartz sand	1.100	38.01
Quartz fume	0.300	10.37
Superplasticizer	0.019	0.66
Water	0.225	7.77

a study on the flexural performance of dovetail wet joints and rectangular wet joints in steel-UHPC composite deck slabs under hogging moment. Chen et al. (Chen et al., 2018) proposed novel interfacial treatments such as epoxy resin treatment and high-pressure water jet chiseling for the wet joints of steel-UHPC composite decks and carried out experiments to study the force mechanism of wet joints. It is recommended that the interfacial treatment using a high-pressure water jet to chisel away the fine aggregate can be used when the construction conditions are suitable. Zhao et al. (Zhao et al., 2018) conducted a full-scale test and finite element simulation study on the flexural performance of dovetail wet joints in steel-RPC composite deck slabs under hogging moment. The test results showed that: reinforcement rate is a key factor affecting crack development and load-deflection curve, and a reinforcement rate of 4.5% is recommended for a 55 mm-thick RPC layer. Lee et al. (Lee et al., 2011) investigated the shear performance and ultimate strength of cast-in-place joints and epoxy adhesive joints in prefabricated UHPC segmental bridges, considering the test parameters such as joint type, load-displacement relationship, fracture behavior, and fracture mode.

However, for the long-span bridges, wet joints are difficult to ensure the quality of joints due to the complex construction process. If the UHPC wet joints are not maintained properly, its mechanical performance will be affected greatly. Epoxy joints have the advantages of good integral performance, better shear bearing capacity than wet joints and lower requirements for maintenance conditions, etc., and have a wider range of adaptation. But the flexural performance of epoxy adhesive joints has been studied quite rarely. Therefore, in this study, four groups of 12 epoxy adhesive prefabricated UHPC bending specimens with different interfacial treatments at their joints were designed to study the bending performance. In addition, a simplified mechanical model of the key-tooth adhesive joint was proposed and a calculation formula for the flexural bearing capacity was established based on the experimental results and theoretical analysis. The research results provide a reference for the study and engineering applications of epoxy adhesive joints of prefabricated UHPC elements.

EXPERIMENTAL PROGRAM

Materials Properties

The main components of UHPC used in this test include cement, silica fume, quartz sand, quartz powder, and straight

steel fibers, and the matrix compound is shown in **Table 1**. The straight steel fiber has a volume ratio of 2%, a length of 8 mm, a diameter of 0.12 mm, and a nominal tensile strength of 2,700 MPa.

The mechanical properties of the UHPC material used in this test are listed in **Table 2**. Among them, the mechanical properties of UHPC were obtained by three 100 mm × 100 mm × 100 mm cubes, three 100 mm × 100 mm × 400 mm bending specimens, three 100 mm × 100 mm × 300 mm prisms, and three dogbone-shaped tensile specimens.

The epoxy resin is CBSR-A/B, which contains the main agent CBSR-A and curing agent CBSR-B, with a ratio of 2:1. According to The methods for properties of resin casting body (GB/T 2567-2021), the mechanical properties of epoxy resin were obtained by tensile and compression tests, as shown in **Figure 1**. The tensile strength, compressive strength, and flexural strength of the epoxy resin are 30 MPa, 100 MPa, and 45 MPa, respectively, and the tensile modulus of elasticity is 3200 MPa.

Design and Production of Specimen

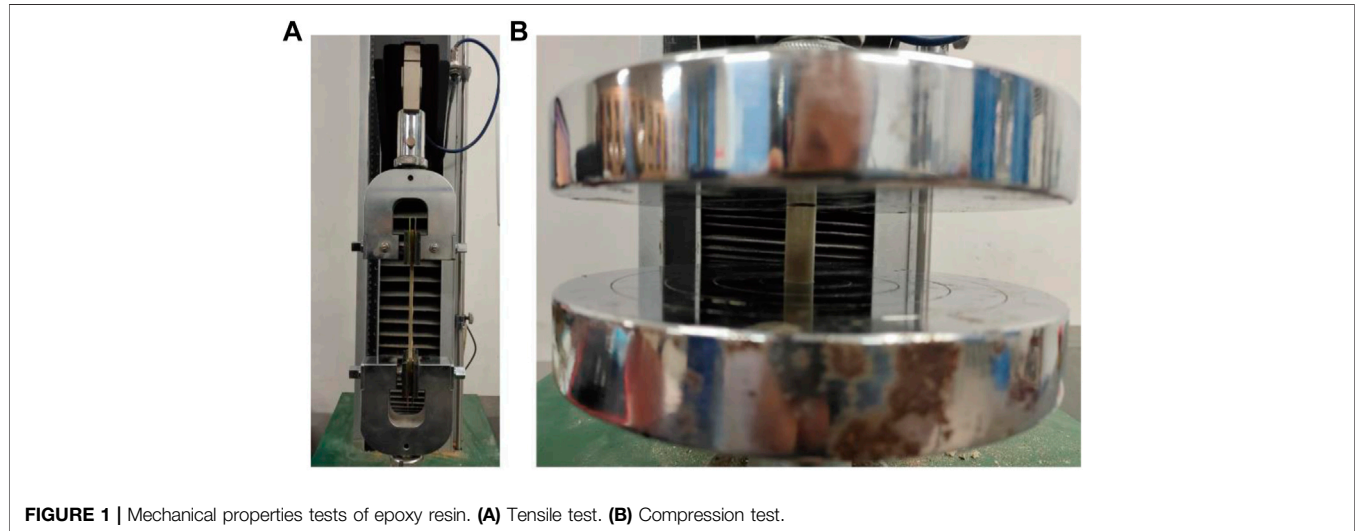
A total of 12 epoxy-adhesive UHPC-UHPC specimens in four groups were designed for this experiment. As shown in **Figure 2**, each specimen consists of two prefabricated UHPC bonded by epoxy resin. The dimension of the single UHPC are 249 mm × 100 mm × 100 mm, and the thickness of the epoxy layer is 2 mm (Zou et al., 2021). The surface at the interface of the two precast UHPC needs to be treated, which can be divided into four types of interfaces according to different treatments: 1) Natural interface, which is a smooth interface made by natural pouring; 2) Rough interface, where the UHPC surface is polished to expose the steel fibers; 3) Groove interface, where four grooves are evenly arranged on the interface, with a single groove size of 2 mm × 10 mm × 100 mm and a groove spacing of 10 mm. 4) Keyway interface. Two keyways were arranged on one side of the prefabricated UHPC interface, the width of the keyway root is 20 mm, the depth is 10 mm, and the spacing of the keyway centerline is 40 mm. The specimens were grouped as listed in **Table 3**.

As shown in **Figure 3**, the specimens were fabricated in sequential steps as follows:

- (1) Making the formwork based on the designed specimen size;
- (2) Pouring the UHPC;
- (3) The specimens were demolded after resting for 3 days in a room with the temperature of $20 \pm 5^\circ\text{C}$ and relative humidity greater than 50%, and the demolded specimens were steam cured for 48 h to ensure that the UHPC reached the design strength;
- (4) The mechanical chiseling of the interface of PD-E-R group specimens until the steel fibers are exposed;
- (5) Applying a 2-mm-thick epoxy resin layer uniformly at the interface of each group specimen and applying normal pressure to form the whole combined UHPC-UHPC specimen;
- (6) Curing all specimens naturally for 7 days to ensure that the epoxy adhesive reaches its design bond strength.

TABLE 2 | Mechanical properties of materials.

Materials	Compressive strength (MPa)	Tensile strength (MPa)	Flexural strength (MPa)	Elastic modulus (GPa)	Poisson's ratio ν_c
UHPC	150	14	20	42.1	0.2

**FIGURE 1** | Mechanical properties tests of epoxy resin. (A) Tensile test. (B) Compression test.

Test Setup and Instrumentation

The loading device is shown in **Figure 4**. The test was carried out using the MTS universal material testing machine with a capacity of 200 kN, and all specimens were loaded by the three-point bending test with a displacement-controlled loading rate of 0.1 mm/min.

The main test items are as follows: 1) Load-deflection curve; 2) Interfacial bending strength; and 3) Final failure modes of the specimen. The load-deflection curve is obtained by the data acquisition system of the MTS universal material testing machine. The interfacial bending strength is calculated by **Eq. 2.1**. The final failure modes of the specimen are observed and recorded at the end of loading.

$$\sigma_{nb} = \frac{3P_n L_m}{2bh^2} \quad (2.1)$$

where σ_{nb} is the interface bending strength, P_n is the ultimate load applied when the interface is damaged, L_m is the distance between the centerline of the two supports, b is the width of the specimen, h is the height of the specimen.

EXPERIMENTAL RESULTS AND DISCUSSION

Interfacial Failure Modes

The two parts of UHPC of each specimen were separated at the end of the test to observe the failure modes at the interface. The failure modes of the interface for a representative specimen of each group are shown in **Figure 5**.

As shown in **Figure 5A**, the interfacial failure modes of PD-E-N series specimens are mainly divided into two parts: the stripping between the epoxy layer-UHPC interface and the damage of the UHPC surface layer. The area outside the red and yellow circles in **Figure 5A** mainly shows the peeling between the epoxy layer-UHPC interface. Both the epoxy layer and UHPC surface are smooth, and no signs of damage are found, indicating that neither is broken by tension. In addition, the area inside the red and yellow circles mainly shows the damage of the UHPC surface layer with a thickness of about 1 mm. The pulled UHPC matrix can be observed on the epoxy surface, which indicates that the bonding performance of the epoxy and UHPC is better, thus leading to the damage of the UHPC surface layer under the tensile stress.

As shown in **Figure 5B**, the interfacial failure modes of PD-E-R series specimens mainly show the pull-out of the UHPC layer on one side of the interface, while the epoxy layer is intact on the other side. The steel fibers and fine aggregates pulled out of UHPC can be observed in the white circle area in **Figure 5B**, this is because some of the exposed steel fibers and fine aggregates are embedded in the epoxy layer, so its bonding performance with the epoxy layer is better. However, the mechanical chiseling treatment of the UHPC surface leads to the damage and loosening of the surface UHPC layer, which causes the interfacial normal tensile strength to be controlled by the loosened UHPC layer.

As shown in **Figure 5C**, the interfacial failure modes of PD-E-G series specimens are similar to that of PD-E-N, which mainly shows the stripping between the epoxy layer-UHPC interface inside the grooves and the damage of the UHPC surface layer

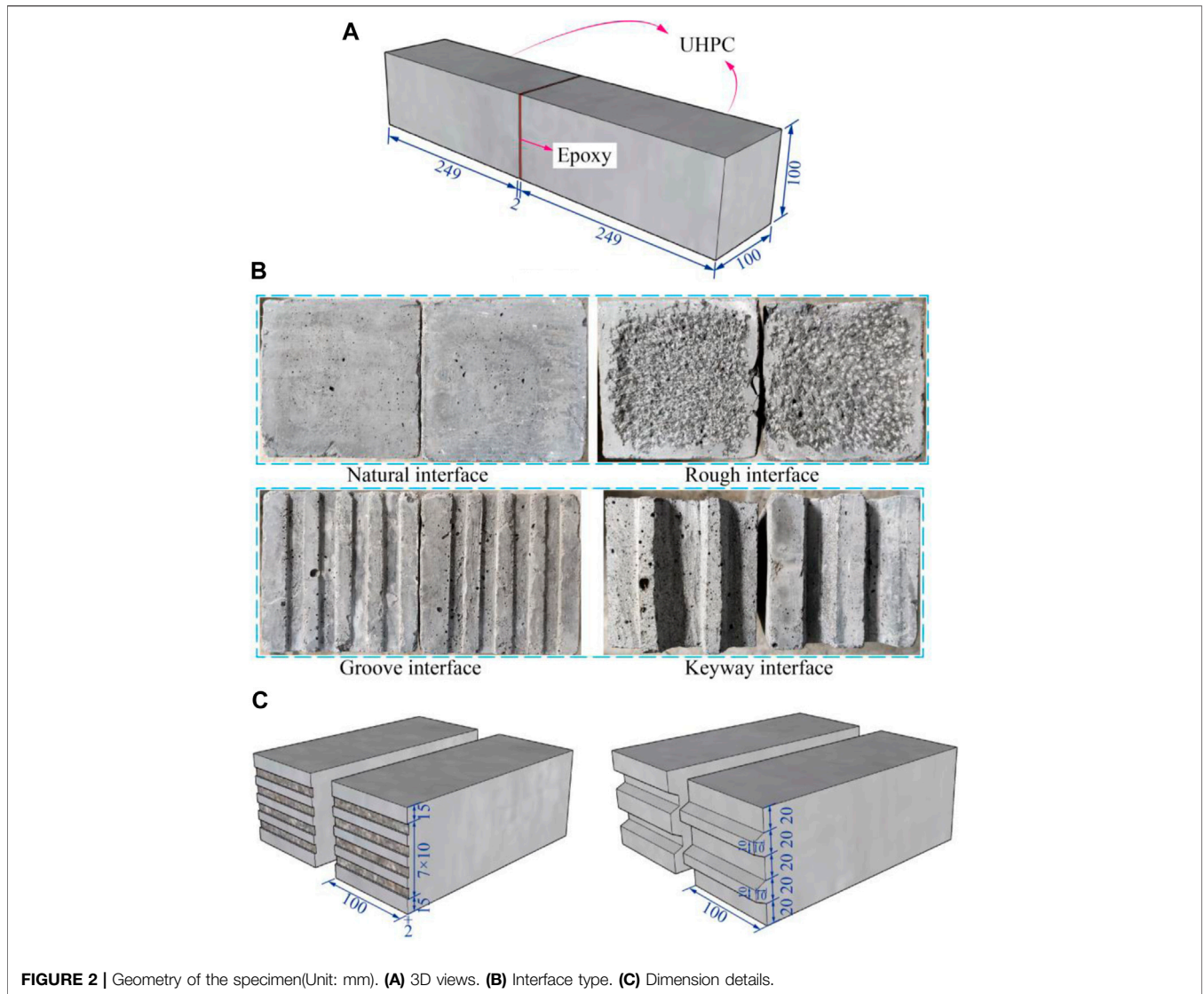


FIGURE 2 | Geometry of the specimen(Unit: mm). **(A)** 3D views. **(B)** Interface type. **(C)** Dimension details.

TABLE 3 | Details of specimens.

Specimen	Number	Surface	Epoxy thick (mm)	Loading mode
PD-E-N-1~3	3	E + N	2	TPB
PD-E-R-1~3	3	E + R	2	TPB
PD-E-G-1~3	3	E + G	2	TPB
PD-E-K-1~3	3	E + K	2	TPB

Note: PD represents prefabricated bridge deck panels, E represents epoxy resin, N, R, G and K represent different interface treatments, and TPB represents three-point Bending loading scheme.

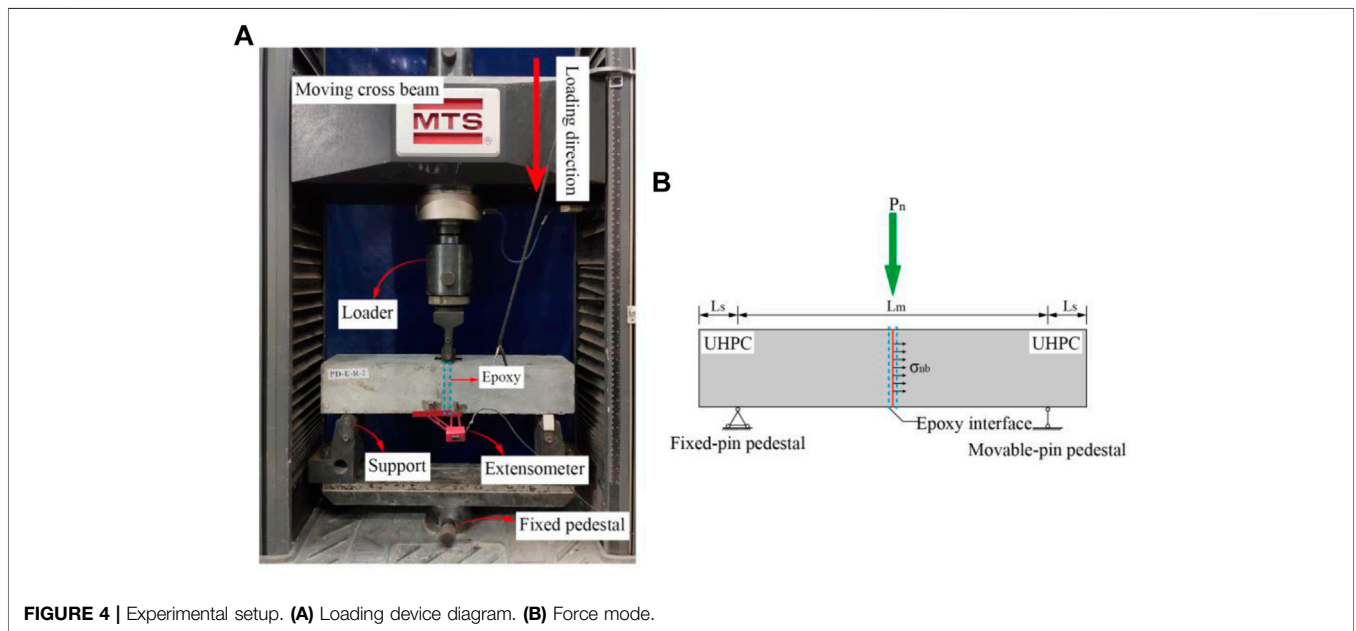
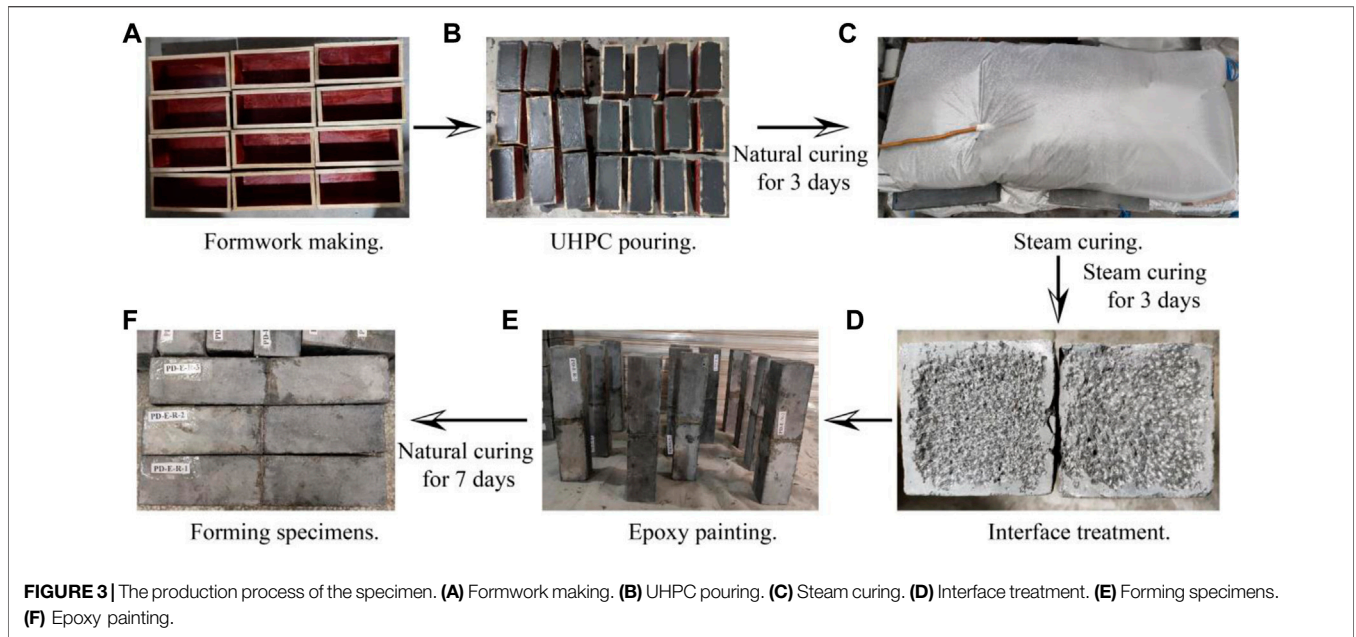
outside the grooves. The epoxy layer and UHPC surface inside the grooves are smooth without damage signs, and they show stripping of the interface and lose the bearing capacity under the normal tension. Compared with the epoxy layer inside the grooves, the thickness of the epoxy layer in the interface area outside the grooves is thinner. Its bonding performance with the

UHPC surface is better, leading to the UHPC surface layer being damaged under normal tension.

As shown in **Figure 5D**, the interfacial failure modes of PD-E-K series specimens mainly show that the UHPC at the root of key teeth on one side is pulled and the interfacial stripping between the epoxy-UHPC surface layer in the area outside the keyway. This indicates that the bonding performance of bonded UHPC-epoxy adhesive interface is excellent after the keyway treatment, and the tensile strength of the interface is controlled by the UHPC near the root of key teeth under normal tension. In addition, after the specimen reaches the ultimate bearing capacity and is damaged, the steel fibers into UHPC limit the development of cracks. The UHPC matrix on both sides of the cracks is not completely separated. The specimen can still bear a certain load and have residual strength.

Interfacial Bond Strength

The test results of this study are summarized in **Table 4** and include the ultimate bearing capacity P_n (kN), interfacial bond



strength σ_{nb} (MPa) and its average value $\sigma_{nb,avg}$ (MPa), mid-span deflection δ_n (mm) and its average value $\delta_{n,avg}$ (mm) when the specimens reach the ultimate load, and residual strength σ_{res} (MPa) and its average value $\sigma_{res,avg}$ (MPa) after the failure of specimens. In this study, the interfacial bond strength σ_{nb} is calculated by Eq. 2.1, the residual strength σ_{res} is the nominal strength of the interface corresponding to the time when the load tends to stabilize after the specimen has reached its ultimate state and is damaged.

To compare the bending resistance of the various interfaces more intuitively way, a comparison of the bending performance of four different interfaces based on Table 4 is shown in Figure 6.

As shown in Figure 6 and Table 4, in descending order of bending strength: the keyway interface, groove interface, natural boundary surface, and rough interface. Compared with the natural interface, the bending tensile strength of rough interface, groove interface, and keyway interface were increased by -24.02, 2.34, and 4.64%, respectively. The bending tensile strength of the rough interface is the lowest among all the treatment methods, because the mechanical chiseling destroys part of the matrix on the UHPC surface. And the looser UHPC layer makes the interface fail under the normal tensile force, and its strength is reduced significantly.

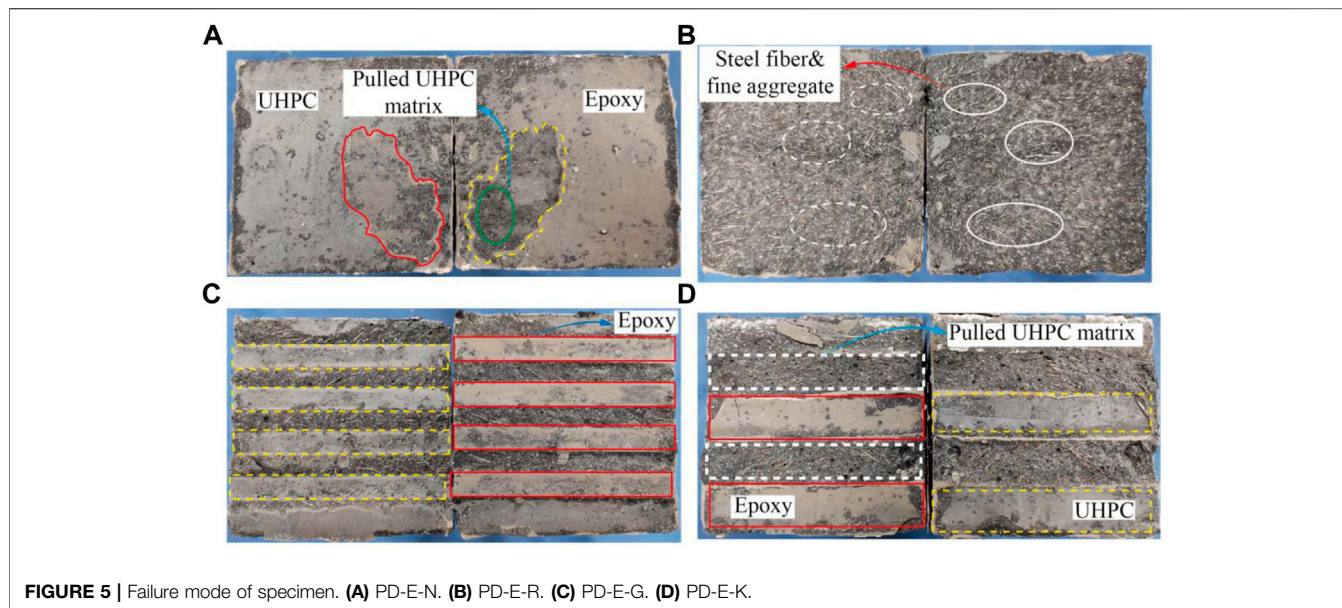


FIGURE 5 | Failure mode of specimen. (A) PD-E-N. (B) PD-E-R. (C) PD-E-G. (D) PD-E-K.

TABLE 4 | The main results of the tests.

Specimens	P_n	σ_{nb}	$\sigma_{nb,avg}$	Difference (%)	δ_n	$\delta_{n,avg}$	Difference (%)	σ_{res}	$\sigma_{res,avg}$	
PD-E-N	PD-E-N-1	17.402	10.441	10.510	0	0.817	0.824	0	0.022	0.015
	PD-E-N-2	18.255	10.953			0.870		0.022		
	PD-E-N-3	16.895	10.137			0.785		0.002		
PD-E-R	PD-E-R-1	14.397	8.638	7.986	-24.02	0.528	0.523	-36.53	0.126	0.279
	PD-E-R-2	12.073	7.244			0.511		0.647		
	PD-E-R-3	13.460	8.076			0.529		0.064		
PD-E-G	PD-E-G-1	17.965	10.779	10.756	2.34	0.732	0.764	-7.28	0.031	0.230
	PD-E-G-2	19.261	11.557			0.807		0.428		
	PD-E-G-3	16.553	9.932			0.752		0.230		
PD-E-K	PD-E-K-1	19.528	11.717	10.998	4.64	0.822	0.789	-4.25	3.930	4.107
	PD-E-K-2	18.569	11.141			0.750		3.828		
	PD-E-K-3	16.895	10.137			0.796		4.563		

Note: The bolded value in the table is the minimum value of column, the underlined bolded value is the maximum value of column, the "Difference" is relative to the specimens with the natural interface (PD-E-N).

Compared with the natural interface, the keyway interface has a more significant increase in bending strength because its failure modes are mainly the tensile damage of UHPC at the root of key teeth. In addition, the deflection at ultimate bending strength is less than 0.83 mm for all four interfaces. The rough interface, groove interface, and keyway interface were reduced by 36.53, 7.28, and 4.25%, respectively, compared to the natural surface. The deflection was also significantly reduced for the rough interface due to its significantly reduced load-carrying capacity.

Furthermore, the natural interface loses its bearing capacity immediately after the failure and has almost no residual strength. Although the rough and groove interfaces have improved compared with the natural surface, their residual strengths are still relatively low, only 0.279 and 0.23 MPa, respectively. However, the keyway interface has a residual strength of 4.107 MPa. It is the only interface with reliable residual strength among the four interfaces. This is because under the action of normal tension, although the UHPC at the root of the keyway is

pulled, the presence of steel fibers limits the rapid development of crack so that the UHPC matrix on both sides of the damaged surface can still bear a certain amount of normal tension under the "connection" of steel fibers, that is, the tensile strength of UHPC after cracking constitutes the residual strength of the specimen.

Load-Deflection Curves

In this study, the load applied to the specimens and the values of mid-span deflection of the specimens were obtained by the sensor acquisition system of the MTS universal material testing machine. The load-deflection curves of four groups of specimens are shown in Figure 7.

As shown in Figure 7A, the load-deflection curves of PD-E-N series specimens exhibit two-fold line form, which is mainly divided into the loading and failure phases. The load rises steadily and almost linearly before the specimen reaches the ultimate load in the loading phase. The curves still maintain high linearity without an obvious yielding phase when the

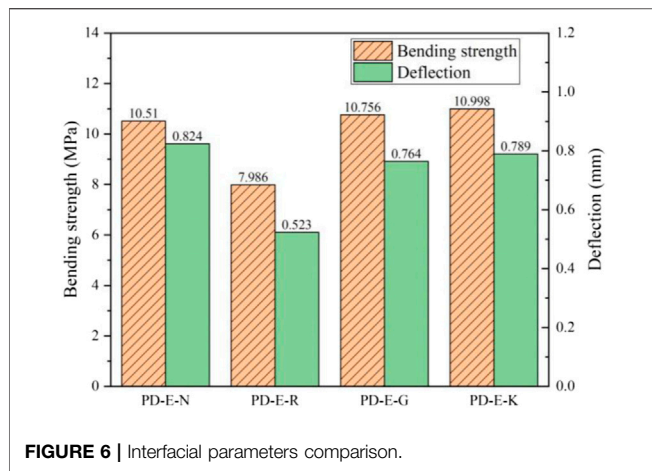


FIGURE 6 | Interfacial parameters comparison.

ultimate bearing capacity is near, which indicates that it does not have ductility. The specimens lose the load-bearing capacity immediately after reaching the ultimate load, without residual strength. This indicates that the interfacial failure belongs to brittle failure, consistent with the failure modes of epoxy layer-UHPC interfacial stripping.

As shown in Figures 7B–D, the general trend of load-deflection curves of the rough interface, groove interface, and keyway interface remains the same as that of the natural interface specimens, all of which mainly show two-fold line form. However, in contrast to the natural surface, the rough and groove interfaces have a certain residual strength after failure. The load shows a slightly increasing trend with the increment of deflection. For the keyway interface, the residual strength is significantly higher than that of the remaining three types of specimens, and the load decreases more slowly with the increment of deflection. This is due to the fact that under the action of normal tension, although the UHPC at the root of the keyway is pulled, the presence of steel fibers limits the rapid development of crack so that the UHPC matrix can still bear a certain amount of normal tension under the “connection” of steel fibers. In conclusion, the ultimate bending tensile strength and residual strength after the failure of the keyway interface are the highest among the four interface forms. The bending performance of the prefabricated UHPC-epoxy adhesive joints is the best when this interface form is adopted.

SIMPLIFIED COMPUTATIONAL METHOD

Force Model and Basic Assumption

The stress state of epoxy adhesive joint is bending-shear composite stress under three-point bending load. Since the tensile strength of epoxy resin is greater than that of UHPC, the bending-shear failure of prefabricated UHPC elements is controlled by the tensile strength of UHPC. The cracks will appear on the UHPC next to the adhesive joint. The calculation diagram is shown in Figure 8.

Since the initial damage and damage area of epoxy resin layer are difficult to define, the following basic assumptions are

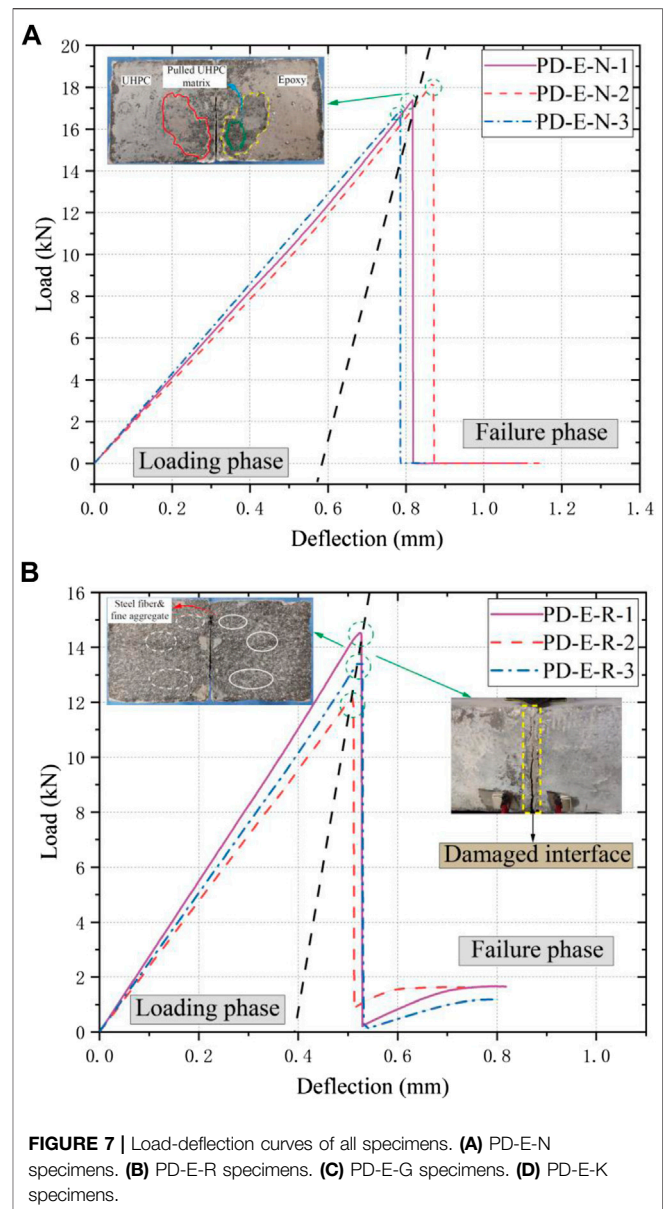


FIGURE 7 | Load-deflection curves of all specimens. (A) PD-E-N specimens. (B) PD-E-R specimens. (C) PD-E-G specimens. (D) PD-E-K specimens.

proposed according to the experimental phenomena to simplify the mechanical behavior of epoxy adhesive joints.

- (1) The joint surface does not crack before reaching the ultimate state, and only the lower half of the adhesive layer cracks after reaching the ultimate state, so the cross-section area of the lower half is only considered when calculating the bearing capacity.
- (2) The adhesive layer loses its bearing capacity after cracking immediately. The residual strength of the specimen is only provided by the bonding force of the upper adhesive layer and UHPC at the root of the key tooth.
- (3) Ignoring the contribution of adhesive layer in key tooth region of cracking zone.
- (4) The dimension of rectangular section is small, so the shear stress on the section is assumed to be uniformly distributed.

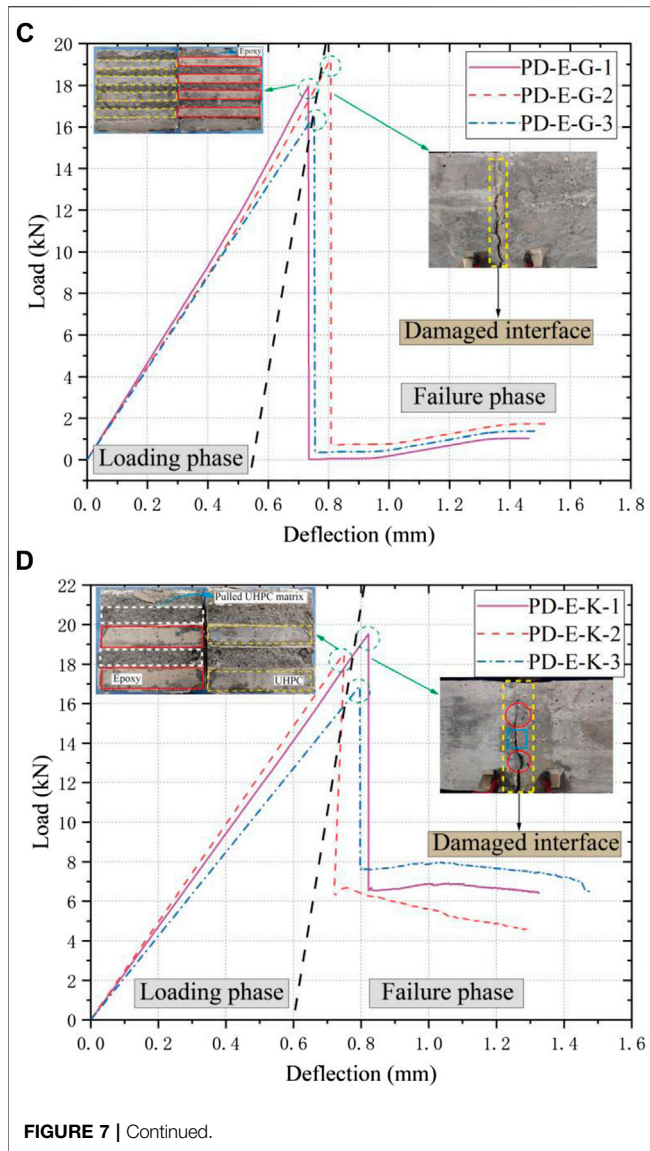


FIGURE 7 | Continued.

Calculation Method of Bearing Capacity

Based on the above basic assumptions and the experimental results of this study, the bearing capacity of the adhesive joint is provided by the bonding force of adhesive layer and UHPC at the root of the key tooth, as shown in Eq. 4.1. The contribution of the adhesive layer can be expressed as follows: Shear slip and normal separation occurred on the joint surface, and the bond strength of the adhesive layer provided resistance load. The adhesive layer begins to damage after the joint surface reaches the maximum bonding strength, and the adhesive layer quits immediately after cracking. It is worth noting that the adhesive layer cracking was observed only in the lower of the specimen, and no cracks were observed in the shear-compression zone under high stress. The failure mode of the key tooth is that the root of key tooth is pulled out under the bending-shear combined action. The adhesive layer of the key tooth region is not cracked,

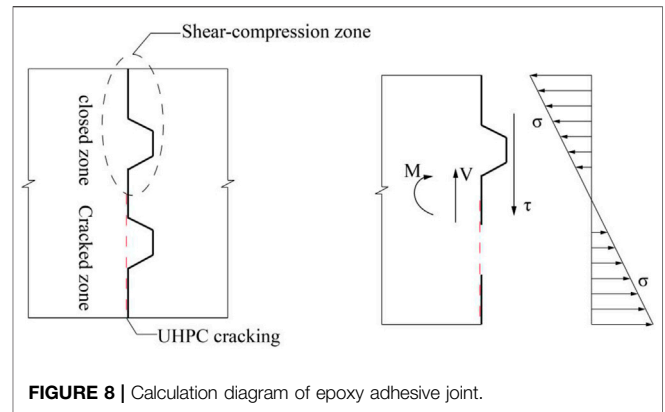


FIGURE 8 | Calculation diagram of epoxy adhesive joint.

so it can be considered that the contribution of the key tooth is only provided by the key tooth matrix itself.

$$P_n = P_a + P_k \tag{4.1}$$

where P_n represents the bearing capacity of adhesive joints, P_a represents the bonding force of adhesive layer, P_k represents the bearing capacity of UHPC at the root of key tooth. The bonding force of the adhesive layer can be obtained from the test results of the adhesive joint with smooth interface. It is worth noting that the tensile strength of UHPC on the surface of specimen and its internal UHPC matrix is quite different due to the different distribution of steel fiber. In this study, the strength reduction coefficient β was introduced to represent the tensile strength of UHPC surface. Therefore, the calculation formula of bonding force is shown in Eq. 4.2:

$$P_a = 4 \frac{\beta f_t W_z}{L_m} \tag{4.2}$$

where f_t represents the uniaxial tensile strength of UHPC, W_z represents the section modulus in bending, L_m represents the calculation span of the prefabricated UHPC elements, β is 0.729 based on the test results of adhesive joints with smooth interface.

For the key teeth, most of the existing study are based on the major principal tensile stress theory (Gopal et al., 2020). The analysis of micro-element of UHPC near the root of the key tooth is shown in Figure 9. From the principle of Mohr's circle, the major principal tensile stress can be obtained as Eq. 4.3:

$$\sigma_1 = \frac{1}{2}(\sigma_x - \sigma_y) + \frac{1}{2}\sqrt{(\sigma_x - \sigma_y)^2 + 4\tau_x^2} \tag{4.3}$$

Since the failure of key teeth is controlled by the tensile strength of UHPC, $\sigma_1 = f_t$, for the ultimate state of bearing capacity, and $\sigma_y = 0$. The calculation formulas of shear stress and normal stress on the rectangular cross-section are shown in Eq. 4.4 and Eq. 4.5, respectively:

$$\tau_x = \frac{3(P_a + P_k)}{2A_k} \tag{4.4}$$

$$\sigma_x = \frac{2(P_a + P_k)L_m}{4W_z} = \frac{(P_a + P_k)L_m}{2W_z} \tag{4.5}$$

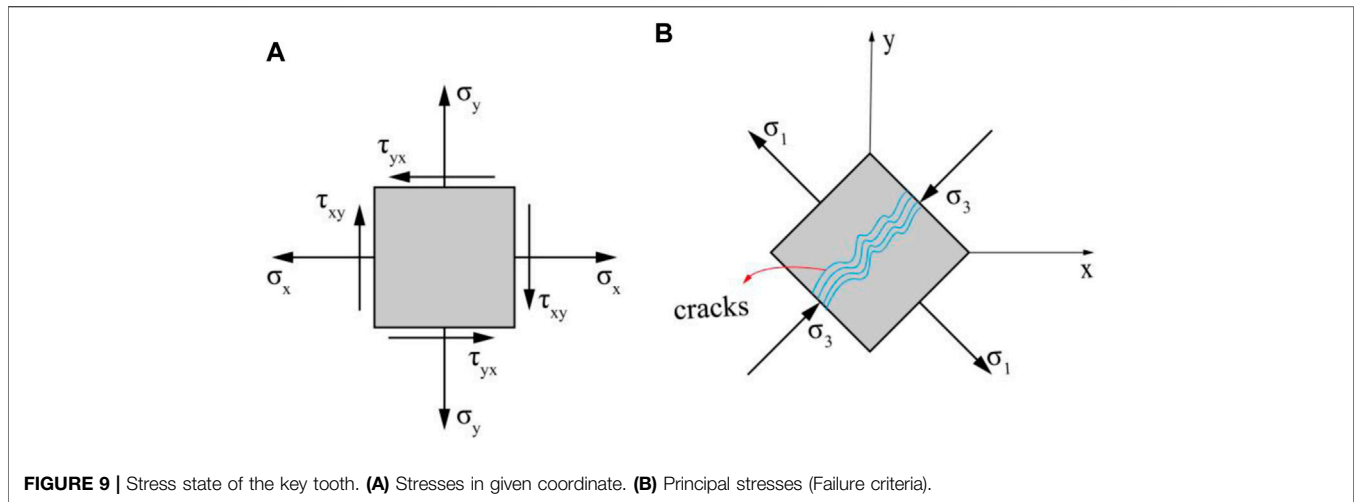


FIGURE 9 | Stress state of the key tooth. **(A)** Stresses in given coordinate. **(B)** Principal stresses (Failure criteria).

where A_k represents the root area of the key tooth. Based on the above formulas, the formula for calculating the bearing capacity of key tooth adhesive joints can be obtained, as shown in Eq. 4.6:

$$P_n = \frac{A_k f_t}{9} \left(\sqrt{\left(\frac{A_k L_m}{W_z} \right)^2 + 36} - \frac{A_k L_m}{W_z} \right) \quad (4.6)$$

In summary, for the smooth adhesive joints, the calculation formula can be expressed as Eq. 4.2 because its bearing capacity is only provided by the bonding force. For the key tooth adhesive joints, the bearing capacity can be expressed as Eq. 4.6.

Comparison of Results

As shown in Table 5, based on the calculation formulas of flexural capacity of epoxy adhesive joints proposed in this study, the smooth adhesive joints and key tooth adhesive joints are calculated, which are compared with the test results.

As can be seen from Table 5, the suggested formulas can better predict the bending capacity of smooth adhesive joints and key tooth adhesive joints. The ratio of calculated value to experimental value is 0.925, and the results are conservative. The standard deviation is 0.065, and the discreteness was small. However, the number of specimens is small in this study relatively, and for the key tooth adhesive joint, the parameters, such as the number and the geometric size of key teeth, are relatively simple. Therefore, the more applicable formula for calculating the bending capacity of key tooth adhesive joints remains to be further studied.

CONCLUSION

To clarify the bending performance of epoxy adhesive joints between prefabricated UHPC elements, the failure modes, load-deflection curves, and interfacial bond strength of prefabricated UHPC epoxy adhesive joints were studied

TABLE 5 | Comparison between calculated and experimental values.

Specimens	No.	P_c	P_n	P_c/P_n
PD-E-N	1	17.01	17.40	0.978
	2	17.01	18.26	0.932
	3	17.01	16.90	1.007
PD-E-K	1	16.02	19.53	0.820
	2	16.02	18.57	0.863
	3	16.02	16.90	0.948
The mean value				0.925
The standard deviation				0.065

Note: P_c represents the calculated values, and P_n represents the test values.

through a three-point bending test. A calculation formula for the flexural bearing capacity was established based on the experimental results and theoretical analysis. The main conclusions are as follows:

- (1) Under the action of normal bending tension, the failure modes of joints with different interface forms vary from each other. The smooth interface mainly shows interfacial stripping failure of the epoxy-UHPC surface layer. A minority of the UHPC surface layer is damaged due to the extraction of steel fibers and fine aggregate. The roughened interface shows interfacial failure due to the pull-out of steel fibers and fine aggregate embedded in epoxy. The groove interface mainly shows the stripping between the epoxy layer-UHPC interface inside the groove and the damage of the UHPC surface layer outside the groove. The keyway interface exhibits tensile damage of UHPC at the root of key teeth and the stripping of epoxy-UHPC surface layer interface in the area outside the keyway.
- (2) The load-deflection curves of all specimens exhibit a two-fold line form, which has no yielding stage before reaching ultimate strength. The mid-span deflection values corresponding to the ultimate strength are lower than

0.83 mm. The interface is instantly damaged after reaching ultimate strength, without sufficient plastic deformation, and exhibits the characteristics of brittle damage.

- (3) Compared with the natural surface, the bending tensile strength of rough interface, grooved interface, and keyway interface were improved by -24.02 , 2.34 , and 4.64% , respectively. Given that the mechanical chiseling method can damage the UHPC surface layer, which in turn reduces the bending strength of the interface, it is recommended to use high-pressure jet technology for the interface roughness treatment. For the keyway interface, which has the most reliable interfacial ultimate and residual strength values among the four groups of specimens, this interfacial form can be adopted for the joints of prefabricated UHPC elements.
- (4) A simplified force model of the keytooth adhesive joint is proposed based on the experimental results and theoretical analysis, and a calculation formula for the flexural bearing capacity is established based on the principal of Mohr's circle. The suggested formulas can better predict the bending capacity of smooth adhesive joints and key tooth adhesive joints. The ratio of calculated value to experimental value is 0.925 , and the results are conservative. The standard deviation is 0.065 , and the discreteness was small.

REFERENCES

- Abdelbaset, H., Cheng, B., Tian, L., Li, H.-T., and Zhang, Q.-H. (2020). Reduce Hot Spot Stresses in Welded Connections of Orthotropic Steel Bridge Decks by Using UHPC Layer: Experimental and Numerical Investigation. *Eng. Structures* 220 (105708), 110988. doi:10.1016/j.engstruct.2020.110988
- Abdelbaset, H., Cheng, B., Tian, L., Li, H.-T., and Zhao, J. (2022). Enhancing Fatigue Resistance of Rib-To-Floorbeam Welded Connections in Orthotropic Steel Bridge Decks by Using UHPC Layer: An Experimental Study. *Structures* 36, 153–167. doi:10.1016/j.istruc.2021.12.008
- Chen, B. C., An, M. Z., Huang, Q. W., Wu, H. C., and Zhao, Q. (2016). "Application of Ultra-High Performance Concrete in Bridge Engineering in China," in First International Interactive Symposium on UHPC, Iowa State University, Des Moines, IA, January 1, 2016 (Des Moines, Iowa, USA: Iowa State University). doi:10.21838/uhpc.2016.82
- Chen, D., Zeng, M., Su, Q., and Lou, Y. (2018). Interfacial Treatment Measures of Wet Joints in Composite Bridge Deck Composed of Steel and UHPC Layer. *China J. Highw. Transport* 31, 154–162. doi:10.19721/j.cnki.1001-7372.2018.12.015
- Cheng, Z., Zhang, Q., Bao, Y., Deng, P., Wei, C., and Li, M. (2021). Flexural Behavior of Corrugated Steel-UHPC Composite Bridge Decks. *Eng. Structures* 246, 113066. doi:10.1016/j.engstruct.2021.113066
- De Larrard, F., and Sedran, T. (1994). Optimization of Ultra-High-Performance concrete by the Use of a Packing Model. *Cement Concrete Res.* 24, 997–1009. doi:10.1016/0008-8846(94)90022-1
- Dieng, L., Marchand, P., Gomes, F., Tessier, C., and Toutlemonde, F. (2013). Use of UHPFRC Overlay to Reduce Stresses in Orthotropic Steel Decks. *J. Constructional Steel Res.* 89, 30–41. doi:10.1016/j.jcsr.2013.06.006
- Du, J., Meng, W., Khayat, K. H., Bao, Y., Guo, P., Lyu, Z., et al. (2021). New Development of Ultra-High-Performance Concrete (UHPC). *Composites B: Eng.* 224, 109220. doi:10.1016/j.compositesb.2021.109220
- Garas, V. Y., Kahn, L. F., and Kurtis, K. E. (2009). Short-Term Tensile Creep and Shrinkage of Ultra-High Performance Concrete. *Cement and Concrete Composites* 31, 147–152. doi:10.1016/j.cemconcomp.2009.01.002

DATA AVAILABILITY STATEMENT

The original contributions presented in the study are included in the article/Supplementary Material, further inquiries can be directed to the corresponding author.

AUTHOR CONTRIBUTIONS

HP conceptualized the study, formulated the methodology, performed the software and formal analysis, and wrote and prepared the original draft. ZZ, YZ, and JG reviewed and edited the manuscript, supervised the study, was in charge of the project administration, and acquired the funding. XZ and XZe conducted data curation. All authors have read and agreed to the published version of the manuscript.

FUNDING

The authors express their sincere gratitude for the financial support provided by the National Natural Science Foundation of China (52008066), the Major Science and Technology Projects in Hainan (ZDKJ2021048), the China Postdoctoral Science Foundation (Grant No. 2021M693919) and Science and technology projects in TAR (XZ202001ZY0054G).

- Gopal, B., Hejazi, F., Hafezolghorani Esfahani, M., and Voo, Y. (2020). Shear Strength of Dry and Epoxy Joints for Ultra-High-Performance Fiber-Reinforced Concrete. *ACI Struct. J.* 117, 279–288. doi:10.14359/51718078
- Haber, Z. B., Munoz, J. F., De la Varga, I., and Graybeal, B. A. (2018). Bond Characterization of UHPC Overlays for Concrete Bridge Decks: Laboratory and Field Testing. *Construction Building Mater.* 190, 1056–1068. doi:10.1016/j.conbuildmat.2018.09.167
- Huang, H., and Ye, G. (2017). Examining the "Time-Zero" of Autogenous Shrinkage in High/Ultra-High Performance Cement Pastes. *Cement Concrete Res.* 97, 107–114. doi:10.1016/j.cemconres.2017.03.010
- Lee, C.-H., Chin, W.-J., Choi, E.-S., and Kim, Y.-J. (2011). An Experimental Study on the Joints in Ultra High Performance Precast Concrete Segmental Bridges. *J. Korea Concrete Inst.* 23, 235–244. doi:10.4334/jkci.2011.23.2.235
- Lee, N. K., Koh, K. T., Park, S. H., and Ryu, G. S. J. C. (2017). Microstructural Investigation of Calcium Aluminate Cement-Based Ultra-high Performance concrete (UHPC) Exposed to High Temperatures. *Cement Concrete Res.* 102, 109–118. doi:10.1016/j.cemconres.2017.09.004
- Li, J., and Deng, Z. (2021). Tensile Behavior of Hybrid Fiber-Reinforced Ultra-High-Performance Concrete. *Front. Mater.* 8, 455. doi:10.3389/fmats.2021.769579
- Lian, J., Hu, C., Fu, T., and Wang, Y. (2021). Review of Self-Sensing Capability of Ultra-High Performance Concrete. *Front. Mater.* 8, 746022. doi:10.3389/fmats.2021.746022
- Liew, J. Y. R. (2015). *Design Guide for Concrete Filled Tubular Members with High Strength Materials to Eurocode 4: Design Guide for Concrete Filled Tubular Members with High Strength Materials to Eurocode*. Lower Kent Ridge Rd, Singapore: Research Publishing, 4.
- Meng, W., Khayat, K. H., and Bao, Y. (2018). Flexural Behaviors of Fiber-Reinforced Polymer Fabric Reinforced Ultra-High-Performance concrete Panels. *Cement and Concrete Composites* 93, 43–53. doi:10.1016/j.cemconcomp.2018.06.012
- Meng, W., and Khayat, K. H. (2018). Effect of Graphite Nanoplatelets and Carbon Nanofibers on Rheology, Hydration, Shrinkage, Mechanical Properties, and Microstructure of UHPC. *Cement Concrete Res.* 105, 64–71. doi:10.1016/j.cemconres.2018.01.001
- Meng, W., and Khayat, K. H. (2017). Improving Flexural Performance of Ultra-High-Performance concrete by Rheology Control of Suspending

- Mortar. *Composites Part B: Eng.* 117, 26–34. doi:10.1016/j.compositesb.2017.02.019
- Pan, W., Fan, J., Nie, J., Hu, J., and Cui, J. (2016). Experimental Study on Tensile Behavior of Wet Joints in a Prefabricated Composite Deck System Composed of Orthotropic Steel Deck and Ultrathin Reactive-Powder Concrete Layer. *J. Bridge Eng.* 21, 04016064. doi:10.1061/(asce)be.1943-5592.0000935
- Qi, J., Bao, Y., Wang, J., Li, L., and Li, W. (2019). Flexural Behavior of an Innovative Dovetail UHPC Joint in Composite Bridges under Negative Bending Moment. *Eng. Structures* 200, 109716. doi:10.1016/j.engstruct.2019.109716
- Qin, F., Zhang, Z., Yin, Z., Di, J., Xu, L., and Xu, X. (2020). Use of High Strength, High Ductility Engineered Cementitious Composites (ECC) to Enhance the Flexural Performance of Reinforced concrete Beams. *J. Building Eng.* 32, 101746. doi:10.1016/j.jobe.2020.101746
- Ren, L., Fang, Z., Zhong, R., and Wang, K. (2019). Experimental and Numerical Investigations of the Seismic Performance of UHPC Box Piers. *KSCE J. Civ Eng.* 23, 597–607. doi:10.1007/s12205-018-0567-8
- Shao, X., Chen, B., and Zhou, X. (2017). Experiment on Bending Behavior of Wet Joints in Light-Weighted Composite Deck System Composed of Steel and RPC Layer. *China J. Highw. Transport* 30, 8. doi:10.19721/j.cnki.1001-7372.2017.03.023
- Shao, X., Qiu, M., Yan, B., Hu, W., and Zhao, X. (2019). Research of High Performance Fabricated Bridge Structures Based on UHPC. *J. Xi'an Univ. Architecture Technology(Natural Sci. Edition)* 51, 8. doi:10.15986/j.1006-7930.2019.02.002
- Shao, X., Yi, D., Huang, Z., Zhao, H., Chen, B., and Liu, M. (2013). Basic Performance of the Composite Deck System Composed of Orthotropic Steel Deck and Ultrathin RPC Layer. *J. Bridge Eng.* 18, 417–428. doi:10.1061/(asce)be.1943-5592.0000348
- Su, J.-z., Ma, X.-l., Chen, B.-c., and Sennah, K. (2019). Full-Scale Bending Test and Parametric Study on a 30-m Span Prestressed Ultra-high Performance concrete Box Girder. *Adv. Struct. Eng.* 23, 1276–1289. doi:10.1177/1369433219894244
- Wang, D., Shi, C., Wu, Z., Xiao, J., Huang, Z., and Fang, Z. (2015). A Review on Ultra High Performance Concrete: Part II. Hydration, Microstructure and Properties. *Construction Building Mater.* 96, 368–377. doi:10.1016/j.conbuildmat.2015.08.095
- Wang, K., Zhao, C., Wu, B., Deng, K., and Cui, B. (2019). Fully-Scale Test and Analysis of Fully Dry-Connected Prefabricated Steel-UHPC Composite Beam under Hogging Moments. *Eng. Structures* 197, 109380. doi:10.1016/j.engstruct.2019.109380
- Wang, Y., Shao, X., Chen, J., Cao, J., and Deng, S. (2021). UHPC-Based Strengthening Technique for Orthotropic Steel Decks with Significant Fatigue Cracking Issues. *J. Constructional Steel Res.* 176, 106393. doi:10.1016/j.jcsr.2020.106393
- Wille, K., Naaman, A., and Parra-Montesinos, G. (2011). Ultra-High Performance Concrete with Compressive Strength Exceeding 150 MPa (22 ksi): A Simpler Way. *ACI Mater. J.* 108, 46–54. doi:10.14359/51664215
- Xiao, J., Guo, L., Nie, J., Li, Y., Fan, J., and Shu, B. (2022). Flexural Behavior of Wet Joints in Steel-UHPC Composite Deck Slabs under Hogging Moment. *Eng. Structures* 252, 113636. doi:10.1016/j.engstruct.2021.113636
- Xue, J., Briseghella, B., Huang, F., Nuti, C., Tabatabai, H., and Chen, B. (2020). Review of Ultra-high Performance Concrete and its Application in Bridge Engineering. *Construction Building Mater.* 260, 119844. doi:10.1016/j.conbuildmat.2020.119844
- Yoo, D.-Y., Park, J.-J., Kim, S.-W., and Yoon, Y.-S. (2014). Influence of Reinforcing Bar Type on Autogenous Shrinkage Stress and Bond Behavior of Ultra High Performance Fiber Reinforced concrete. *Cement and Concrete Composites* 48, 150–161. doi:10.1016/j.cemconcomp.2013.11.014
- Zhang, Z., Liu, D., Ding, Y., and Wang, S. (2022). Mechanical Performance of Strain-Hardening Cementitious Composites (SHCC) with Bacterial Addition. *J. Infrastructure Preservation Resilience* 3, 3. doi:10.1186/s43065-022-00048-3
- Zhang, Z., Liu, S., Yang, F., Weng, Y., and Qian, S. (2021). Sustainable High Strength, High Ductility Engineered Cementitious Composites (ECC) with Substitution of Cement by rice Husk Ash. *J. Clean. Prod.* 317, 128379. doi:10.1016/j.jclepro.2021.128379
- Zhang, Z., Yang, F., Liu, J.-C., and Wang, S. (2020). Eco-Friendly High Strength, High Ductility Engineered Cementitious Composites (ECC) with Substitution of Fly Ash by rice Husk Ash. *Cement Concrete Res.* 137, 106200. doi:10.1016/j.cemconres.2020.106200
- Zhao, C., Wang, K., Zhou, Q., Deng, K., and Cui, B. (2018). Full-Scale Test and Simulation on Flexural Behavior of Dovetail-Shaped Reactive Powder-Concrete Wet Joint in a Composite Deck System. *J. Bridge Eng.* 23, 04018051. doi:10.1061/(asce)be.1943-5592.0001265
- Zhou, M., Lu, W., Song, J., and Lee, G. C. (2018). Application of Ultra-High Performance Concrete in Bridge Engineering. *Construction Building Mater.* 186, 1256–1267. doi:10.1016/j.conbuildmat.2018.08.036
- Zhu, J.-S., Wang, Y.-G., Yan, J.-B., and Guo, X.-Y. (2020). Shear Behaviour of Steel-UHPC Composite Beams in Waffle Bridge Deck. *Compos. Structures* 234, 111678. doi:10.1016/j.compstruct.2019.111678
- Zou, Y., Jiang, J., Zhou, Z., Wang, X., Guo, J., and Zhang, Z. (2021). Study on the Static Performance of Prefabricated UHPC-Steel Epoxy Bonding Interface. *Adv. Civil Eng.* 2021, 1–15. doi:10.1155/2021/6663517

Conflict of Interest: The authors declare that the research was conducted in the absence of any commercial or financial relationships that could be construed as a potential conflict of interest.

Publisher's Note: All claims expressed in this article are solely those of the authors and do not necessarily represent those of their affiliated organizations, or those of the publisher, the editors and the reviewers. Any product that may be evaluated in this article, or claim that may be made by its manufacturer, is not guaranteed or endorsed by the publisher.

Copyright © 2022 Peng, Zhang, Zou, Guo, Zhang and Zeng. This is an open-access article distributed under the terms of the Creative Commons Attribution License (CC BY). The use, distribution or reproduction in other forums is permitted, provided the original author(s) and the copyright owner(s) are credited and that the original publication in this journal is cited, in accordance with accepted academic practice. No use, distribution or reproduction is permitted which does not comply with these terms.